Supplement of The Cryosphere, 18, 525–541, 2024
https://doi.org/10.5194/tc-18-525-2024-supplement

The Cryosphere Open Access EGU

Supplement of

Seasonal to decadal dynamics of supraglacial lakes on debris-covered glaciers in the Khumbu region, Nepal

Lucas Zeller et al.

Correspondence to: Lucas Zeller (lucas.zeller@colostate.edu)

Supplement

S1 Planet: Data access and cleanup

Imagery covering the AOI was searched for and downloaded using the Planet Orders API (Planet Team 2017). For each glacier, we selected images that (1) captured the entire glacier extent, (2) had less than 15% cloud cover across the entire image, and (3) contained four-band (RGB and near-infrared (NIR)), ortho-rectified, surface-reflectance data (the "ortho_analytic_4b_sr" asset type). We additionally included pairs of images which were taken by the same satellite on the same day that, when combined, captured the entire glacier surface and each met criteria (2) and (3). A full list of all images meeting these criteria was compiled for the eight study glaciers. The 'harmonize' tool was used when ordering these images using the Planet Orders API. This tool brings the spectral response of each image in line with coincident Sentinel-2 imagery, ensuring a consistent spectral response across the multitude of individual sensors.

This entire image collection was downloaded to a local computer for additional processing and lake identification. For each glacier, images were merged together (if needed) and then clipped to the AOI extent. Each image was then manually inspected to ensure suitable data quality. Images with considerable cloud cover or snow cover, anomalous spectral responses, or poor band coregistration were discarded.

Areas of cloud cover and terrain shadows were identified in each image and excluded from future analysis. Cloud-covered areas were classified using the Planet-provided usable data mask. We developed an approach to identify terrain shadows within PlanetScope images as dark, spatially-continuous areas (described in detail below).

S2 Planet: Shadow Masking

A novel texture-based approach was developed to identify and mask out terrain shadowing in PlanetScope images. Shadows were identified on the glacier surface as large, continuous areas that were dark and had little spatial variation in brightness. These areas were identified using a multi-step process. First, areas of very high confidence shadow (shadow "seeds") were identified. These were identified if it met the following criteria:

1. The average surface brightness in visible bands was less than 1000 (using the image digital numbers).
2. At least 75% of on-glacier pixels within 99 meters had surface brightness less than 1000
3. The standard deviation of surface brightness of pixels within 99 meters was less than 50

These areas of shadow seeds were then iteratively expanded to include the continuous regions surrounding them with pixel brightness below the 1000 DN threshold in visible bands, with small voids and gaps filled.

S3 Planet: Filtering and smoothing

A pixel-wise temporal smoothing algorithm was applied to the initial water classification images to prevent individual pixels from rapidly switching between being classified as water and non-water. For each pixel, we collated the time series of all observations across the 2017–2022 period. Individual observations were assigned a value of 1 if the pixel was identified as water and 0 if it was not. A Gaussian filter was then applied to this time series, using a Gaussian kernel with a standard deviation of 14 days. For each point, if the resulting smoothed value was greater than or equal to 50% of the potential maximum value (the value it would be if all observations were initially classified as water) then that pixel in that image was given a "smoothed" classification of water. All other observations were classified as non-water. The products at the end of this smoothing process (Figure 2d, Temporally Smoothed Water) represent the spatiotemporal distribution of unfrozen SGLs.

The temporally smoothed water products were then used to further constrain the classification of frozen lake surfaces (Figure 2d, Spatiotemporal Ice Masking). Each pixel which was initially classified as lake ice remained as a lake ice pixel only if it was also classified as water at any point within the preceding or following 60 days (resulting in the Filtered Ice product). This limited the mis-classification of snow drifts and ice cliffs as SGLs. Finally, the filtered ice dataset was combined with the temporally smoothed water dataset, and the same Gaussian temporal smoothing was applied to this combined dataset, resulting in the final lake extent dataset. This provides the extent of all lakes, including frozen and unfrozen, within each image.

S4 Landsat Glacier Ice Masking

Continuously exposed areas of glacier ice in Landsat images were identified using thresholding on the normalized difference snow index (NDSI) and blue band surface reflectance. As a first step, areas of snow/ice were identified as pixels with an NDSI value greater than 0.2 and blue reflectance greater than 0.35. In order to avoid mis-classifying temporary snow cover, ice cliffs, or frozen lake surfaces as glacier ice we then applied a temporal smoothing to these products. For each Landsat image, pixels were given a final classification of glacier ice if that pixel was identified as ice using the aforementioned thresholds in greater than 60% of all Landsat images captured within the surrounding four years (two years before and after). These final glacier ice extents were then excluded from being classified as water. A final filtering step was also applied to remove occasional linear artifacts in Landsat 5 near-infrared bands. Pixels where the difference between the green and near infrared reflectance (green minus near-infrared) was greater than 0.2 were masked out and not included in the analysis.

Table S1. Physical characteristics of each of the eight glaciers investigated. Note that all columns, other than "Total Glacier Size" refer to only the areas of investigation (AOI) used in this study. Ice flow velocities are given by the mean plus/minus one standard deviation. Note that Imja and Lhotse Shar (*) are considered a single glacier in RGI 6.0 (RGI Consortium, 2017). Debris thicknesses were taken from Rounce et al. (2021), and flow velocities were taken from NASA ITS_LIVE velocity mosaics (Gardner et al., 2022)

Glacier	Debris-covered Area (km^2, within AOI)	Total Glacier Size (km^2, RGI 6.0)	Glacier Length (km, within AOI)	Average debris thickness (m, within AOI)	Flow velocity (m yr^{-1}, within AOI)
Ama Dablam	2.23	4.82	3.87	1.04	0.76 $\pm$0.96
Ambulapcha	0.91	1.92	1.72	0.51	0.82 $\pm$0.40
Imja	1.01	14.27*	1.59	0.20	1.38 $\pm$1.39
Khumbu	5.74	19.10	8.09	0.82	1.53 $\pm$2.97
Lhotse	5.21	6.83	5.81	0.13	3.30 $\pm$6.06
Lhotse Nup	1.60	2.84	3.54	0.44	1.02 $\pm$1.25
Lhotse Shar	3.21	14.27*	3.41	0.43	3.35 $\pm$4.40
Nuptse	2.77	3.69	5.20	0.33	3.05 $\pm$4.07

Table S2. Number of images for each glacier from each source, after manual filtering of images with cloud cover, snow cover, or poor image quality.

Glacier	Planet	Landsat 5	Landsat 7	Landsat 8	Landsat 9	Sentinel-2
Pre-filtering		324	394	204	20	288
Ama Dablam	495	148	174	91	6	83
Ambulapcha	467	139	169	98	10	95
Imja	411	167	190	113	12	111
Khumbu	306	174	0	104	9	108
Lhotse	371	153	181	89	10	101
Lhotse Nup	468	162	209	97	12	112
Lhotse Shar	338	160	183	96	13	116
Nuptse	422	160	173	92	9	115

Table S3. Error statistics for Landsat and Sentinel-2 SGL identification on each glacier. Presented as the median per-image difference in SGL area across all validation imagery for each glacier (MAE, in m^2), and then normalized by image-specific SGL (as %). Bias is computed by subtracting Landsat/Sentinel-2 derived SGL area from PlanetScope-derived area.

	Landsat 7 & 8		Sentinel-2	
Glacier	MAE (m^2 and %)	Bias (m^2 and %)	MAE (m^2 and %)	Bias (m^2 and %)
Ama Dablam	4752 (49.7%)	-207 (-1.3%)	2915 (26.3%)	648 (4.1%)
Ambulapcha	1994 (21.2%)	-572 (-4.3%)	2505 (13.0%)	-1996 (-11.4%)
Imja	940 (100.0%)	-828 (-61.7%)	264 (59.9%)	-233 (-23.2%)
Khumbu	31797 (19.8%)	-22950 (-14.2%)	48391 (30.7%)	-48391 (-30.1%)
Lhotse	11475 (19.2%)	4149 (+4.4%)	17441 (25.7%)	-5562 (-6.1%)
Lhotse Nup	3285 (55.1%)	-3285 (-36.8%)	2223 (38.1%)	-1371 (-19.7%)
Lhotse Shar	11016 (36.8%)	-10809 (-28.1%)	14422 (44.0%)	-12512 (-31.5%)
Nuptse	10143 (35.6%)	-10143 (-30.8%)	11345 (40.1%)	-11345 (-40.7%)
Overall	5436 (36.8%)	-2079 (-23.6%)	5796 (34.3%)	-2618 (-21.6%)

Table S4. Lake number and area minimums (min.) and maximums (max.) for each glacier in 2018.

Glacier	2018 min. (#)	2018 max. (#)	2018 min. (area)	2018 max (area)
Ama Dablam	18	72	22563	57555
Ambulapcha	4	35	9081	35658
Imja	4	23	612	4464
Khumbu	176	646	162414	268362
Lhotse	82	402	74124	204399
Lhotse Nup	17	65	9189	22626
Lhotse Shar	44	272	26739	91449
Nuptse	33	125	34047	59337

Table S5. Lake number and area minimums (min.) and maximums (max.) for each glacier in 2019.

Glacier	2019 min. (#)	2019 max. (#)	2019 min. (area)	2019 max (area)
Ama Dablam	31	85	29016	54441
Ambulapcha	6	42	17244	35739
Imja	3	18	549	4455
Khumbu	157	690	163863	363519
Lhotse	86	399	128691	207162
Lhotse Nup	18	67	10494	22554
Lhotse Shar	43	285	28710	69687
Nuptse	34	118	35406	48906

Table S6. Lake number and area minimums (min.) and maximums (max.) for each glacier in 2020.

Glacier	2020 min. (#)	2020 max. (#)	2020 min. (area)	2020 max (area)
Ama Dablam	30	92	14382	36279
Ambulapcha	12	64	17262	55755
Imja	1	31	855	6498
Khumbu	165	572	183492	275481
Lhotse	103	442	54405	172557
Lhotse Nup	14	97	4131	29007
Lhotse Shar	48	318	29547	97596
Nuptse	30	138	33264	84213

Table S7. Lake number and area minimums (min.) and maximums (max.) for each glacier in 2021.

Glacier	2021 min. (#)	2021 max. (#)	2021 min. (area)	2021 max (area)
Ama Dablam	10	73	7641	49788
Ambulapcha	9	33	20304	36405
Imja	0	18	0	2448
Khumbu	115	405	164619	436536
Lhotse	79	292	63693	276912
Lhotse Nup	9	54	3465	14625
Lhotse Shar	45	188	26190	171522
Nuptse	22	112	32526	82215

Table S8. Lake number and area minimums (min.) and maximums (max.) for each glacier in 2022.

Glacier	2022 min. (#)	2022 max. (#)	2022 min. (area)	2022 max (area)
Ama Dablam	40	112	23940	51534
Ambulapcha	18	44	27927	46323
Imja	3	26	729	5076
Khumbu	218	563	223605	306729
Lhotse	120	340	94023	170064
Lhotse Nup	29	82	7803	34578
Lhotse Shar	64	242	22626	85770
Nuptse	39	138	45765	66618

Table S9. Long-term trends in SGL area on each glacier, as seen in Landsat-derived SGL products. Trends are presented as the lake area change per year from linear regression analysis of the entire timeframe (1988-2022) as well as only for the 2013-2022 period. Results are further broken down by glacier-wide lake area trends near-terminus (lower 50% by distance from terminus) trends. P-values are provided for each.

Glacier	Full Glacier 1988–2022 $m^2\ yr^{-1}$ (P-value)	Full Glacier 2013–2022 $m^2\ yr^{-1}$ (P-value)	Terminus only 1988–2022 $m^2\ yr^{-1}$ (P-value)	Terminus only 2013–2022 $m^2\ yr^{-1}$ (P-value)
Ama Dablam	128 (0.355)	-1156 (0.117)	34 (0.587)	-1143 (0.025)
Ambulapcha	294 (0.000)	687 (0.204)	249 (0.000)	1135 (0.003)
Imja	-109 (0.004)	25 (0.500)	-112 (0.001)	0 (1.000)
Khumbu	2413 (0.000)	8348 (0.001)	2678 (0.000)	12745 (0.000)
Lhotse	-192 (0.740)	2212 (0.302)	382 (0.152)	5408 (0.002)
Lhotse Nup	-118 (0.107)	-104 (0.757)	-15 (0.587)	-155 (0.340)
Lhotse Shar	-1971 (0.001)	-1860 (0.194)	-258 (0.025)	-286 (0.538)
Nuptse	155 (0.227)	674 (0.271)	329 (0.000)	1045 (0.084)

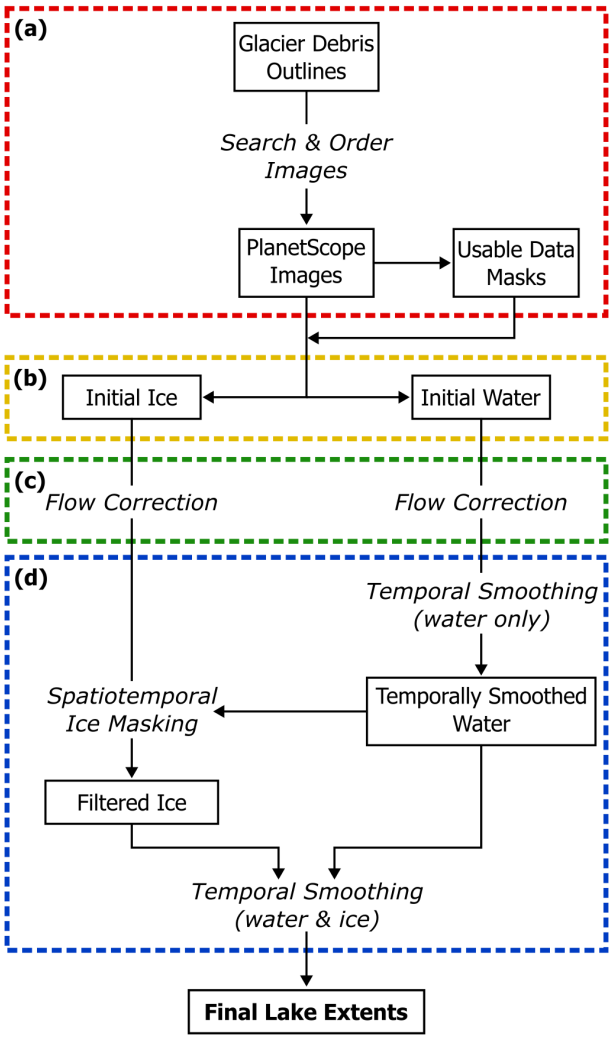

Figure S1. Workflow diagram for delineating supraglacial lakes in PlanetScope imagery. The boxed items indicate intermediate products in the workflow, while unboxed, italicized labels indicate processing steps which are referred to in the text.

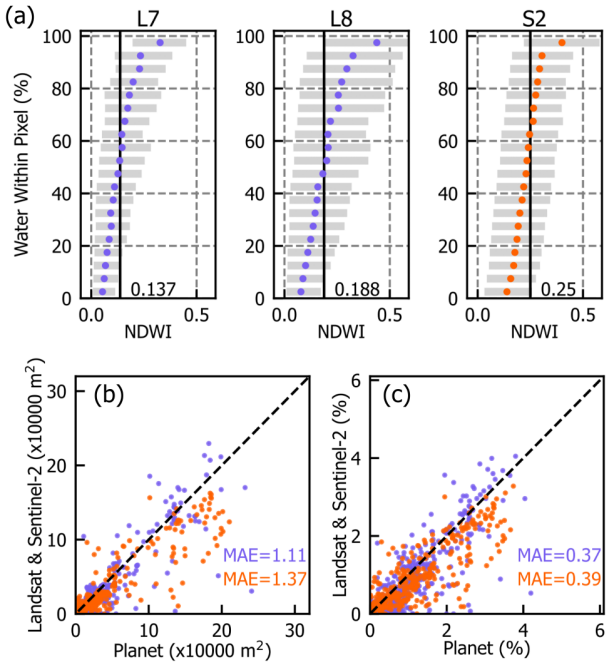

Figure S2. (a) NDWI optimization results for each satellite. Each horizontal bar shows the range of NDWI values for Landsat and Sentinel-2 pixels in the validation dataset with the indicated percent water cover (aggregated in 5% bins). Dots indicate the mean, grey bars show the range containing 90% of all observations. Vertical lines and the shown number indicate the optimized NDWI value for each sensor, which minimized the net error over the validation dataset. (b) and (c) compare the SGL area identified in PlanetScope imagery and in Landsat/Sentienel-2 coincident imagery using the optimized thresholds, with each point representing a single image. (b) shows these values as the total lake area, while (c) scales them by the total glacier debris-covered area. Mean absolute error (MAE) is shown for Landsat (purple) and Sentinel-2 (orange) results on each plot.

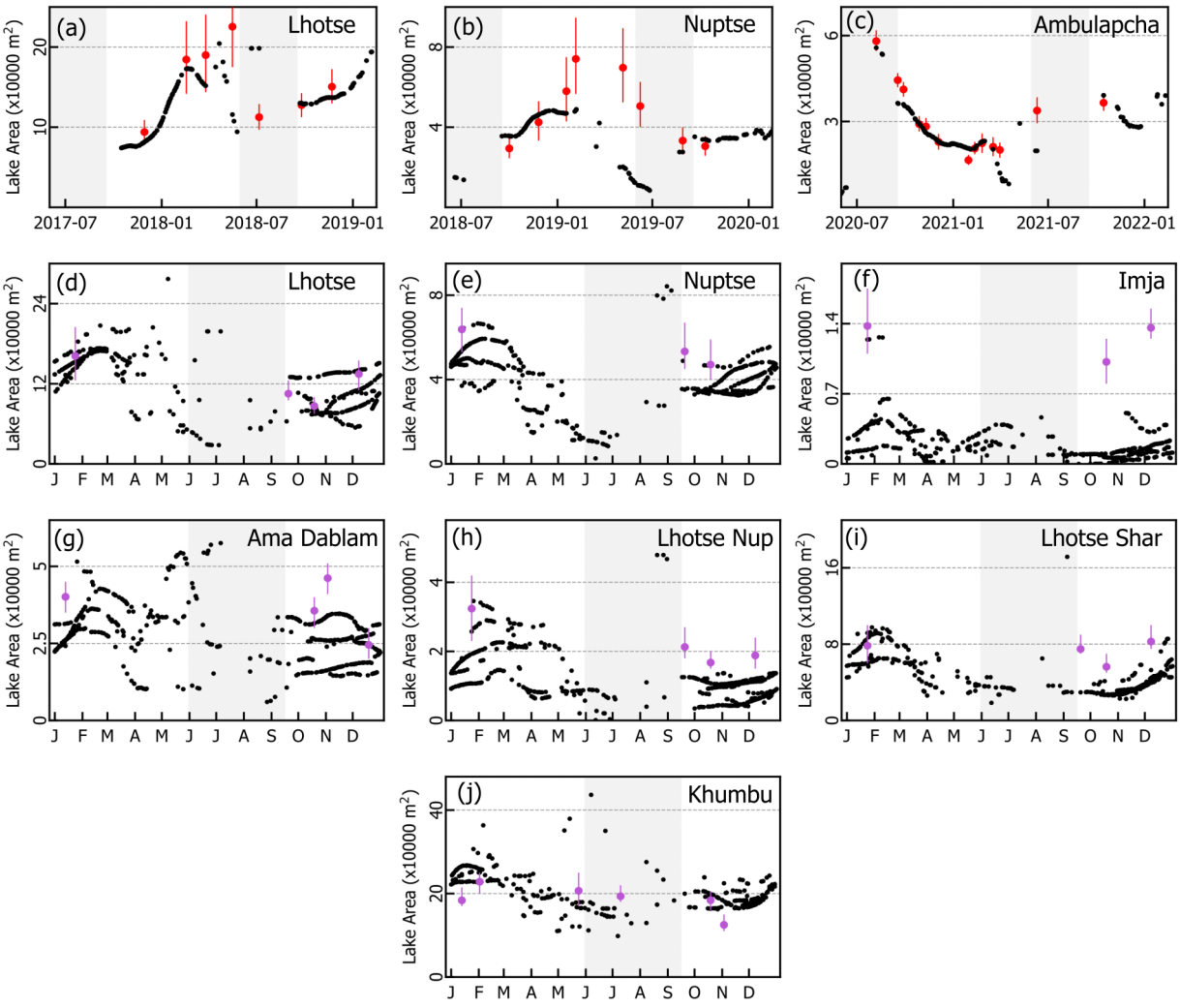

Figure S3. a-c) A comparison of automated lake areas (black dots) to the manually-delineated validation images on Lhotse, Nuptse, and Ambulapcha Glaciers (red). d-j) Comparison between automated lake areas and results from Watson et al. (2016, purple). Comparisons with Watson et al. are presented with results plotted by day of year (tick labels indicating the beginning of each month), as there was no temporal overlap between our observations and theirs. Grey shaded areas indicate monsoon months. Red and purple bars indicate error estimates from a ± 1 pixel buffering.

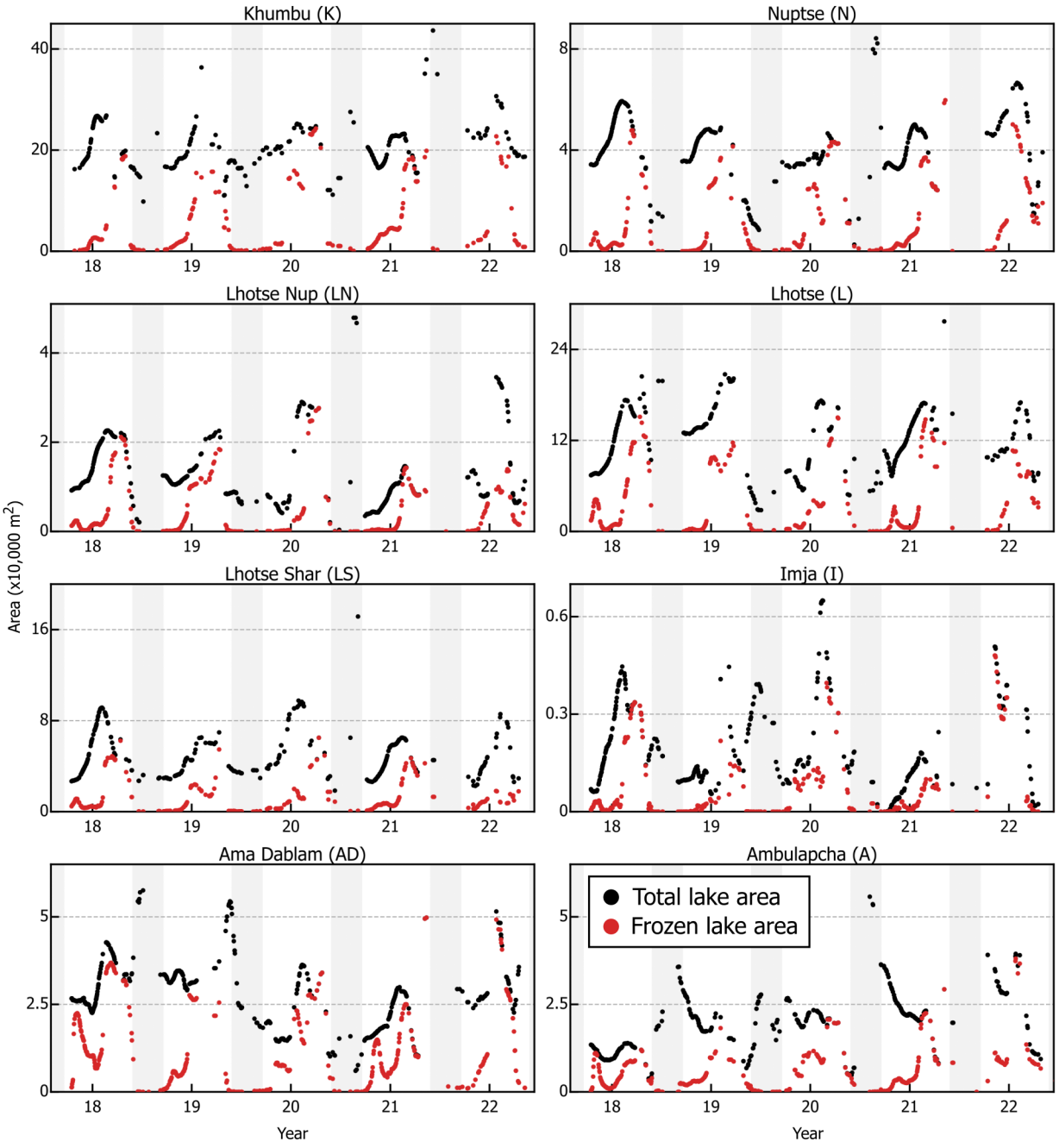

Figure S4. Comparison of the timeseries of total lake area (black points) and the total area of lake surface which are frozen (red points) for each glacier across the five-year study period.

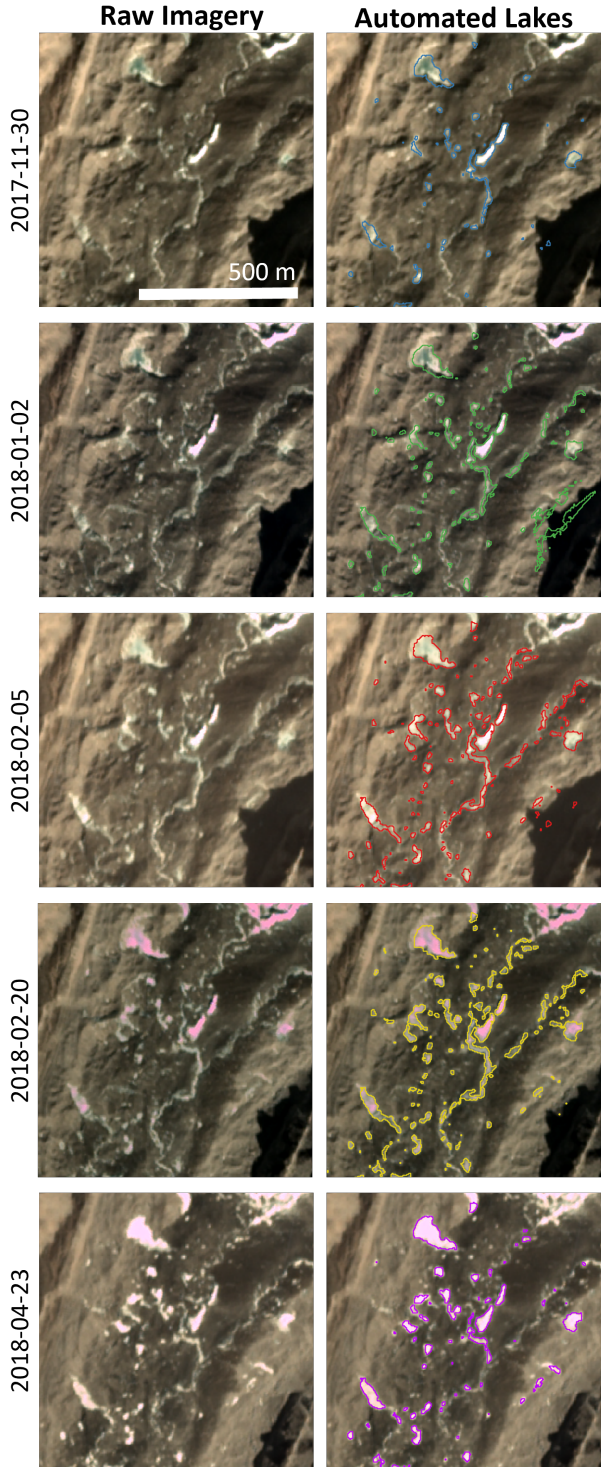

Figure S5. An example of the SGL changes in the upper region of Khumbu Glacier between November 2017 and April 2018. Outlines show the automated SGL identification.

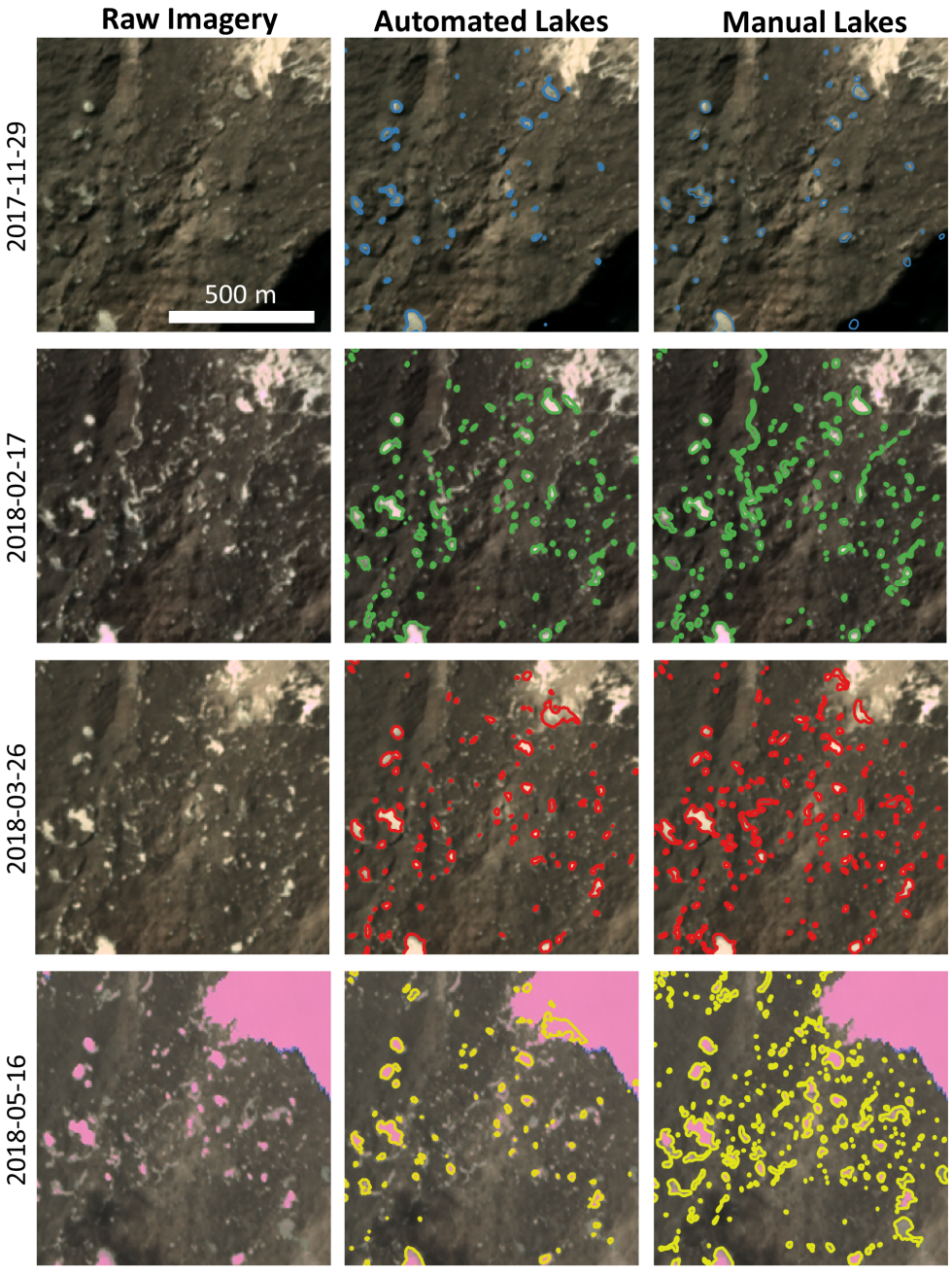

Figure S6. An example of the SGL changes in the upper region of Lhotse Glacier between November 2017 and May 2018. Center outlines show the automated SGL identification, left outlines show the manual validation dataset outlines.

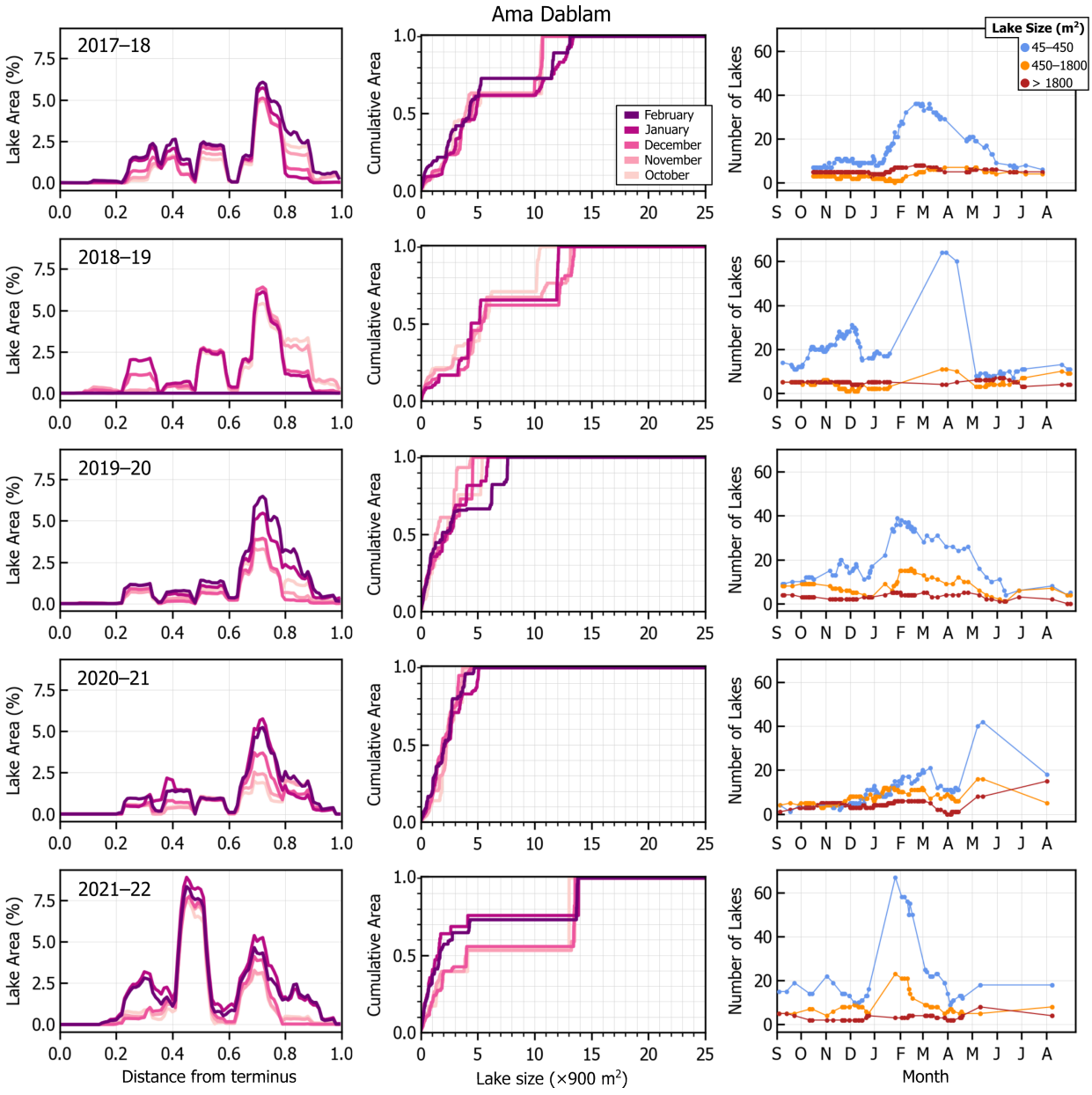

Figure S7. Seasonality in lake area and count on Ama Dablam Glacier, presented identically as Figure 6.

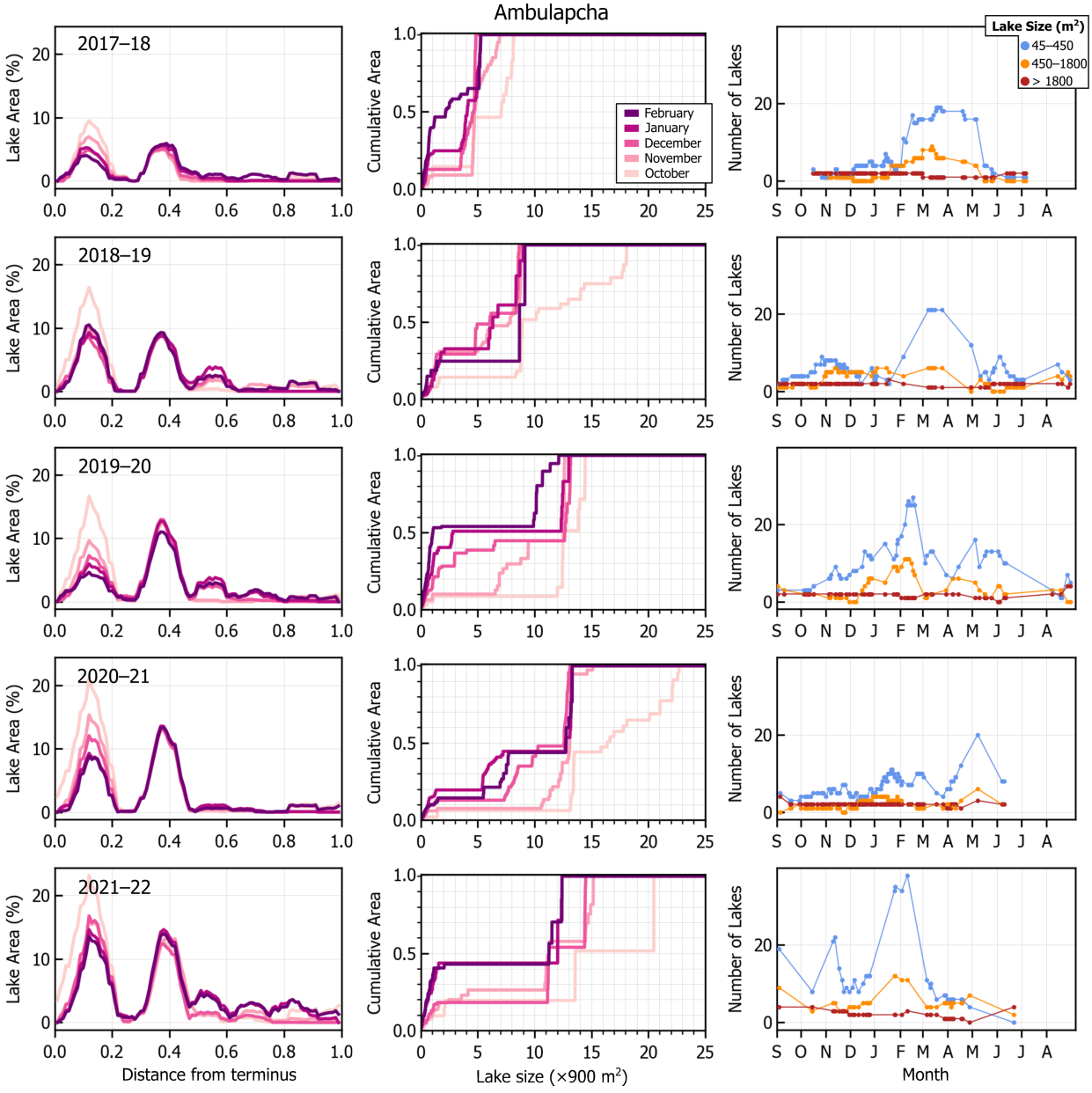

Figure S8. Seasonality in lake area and count on Ambulapcha Glacier, presented identically as Figure 6.

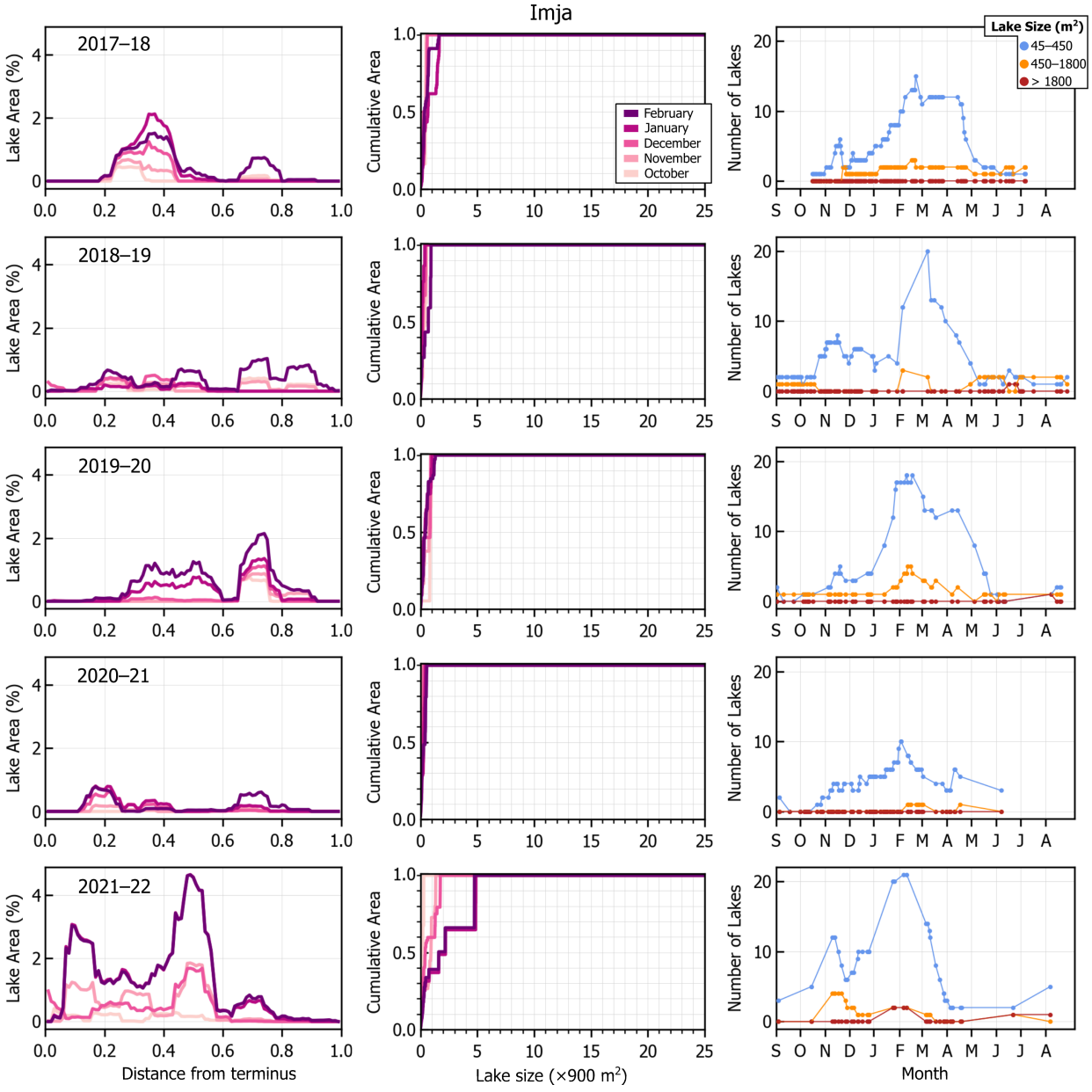

Figure S9. Seasonality in lake area and count on Imja Glacier, presented identically as Figure 6.

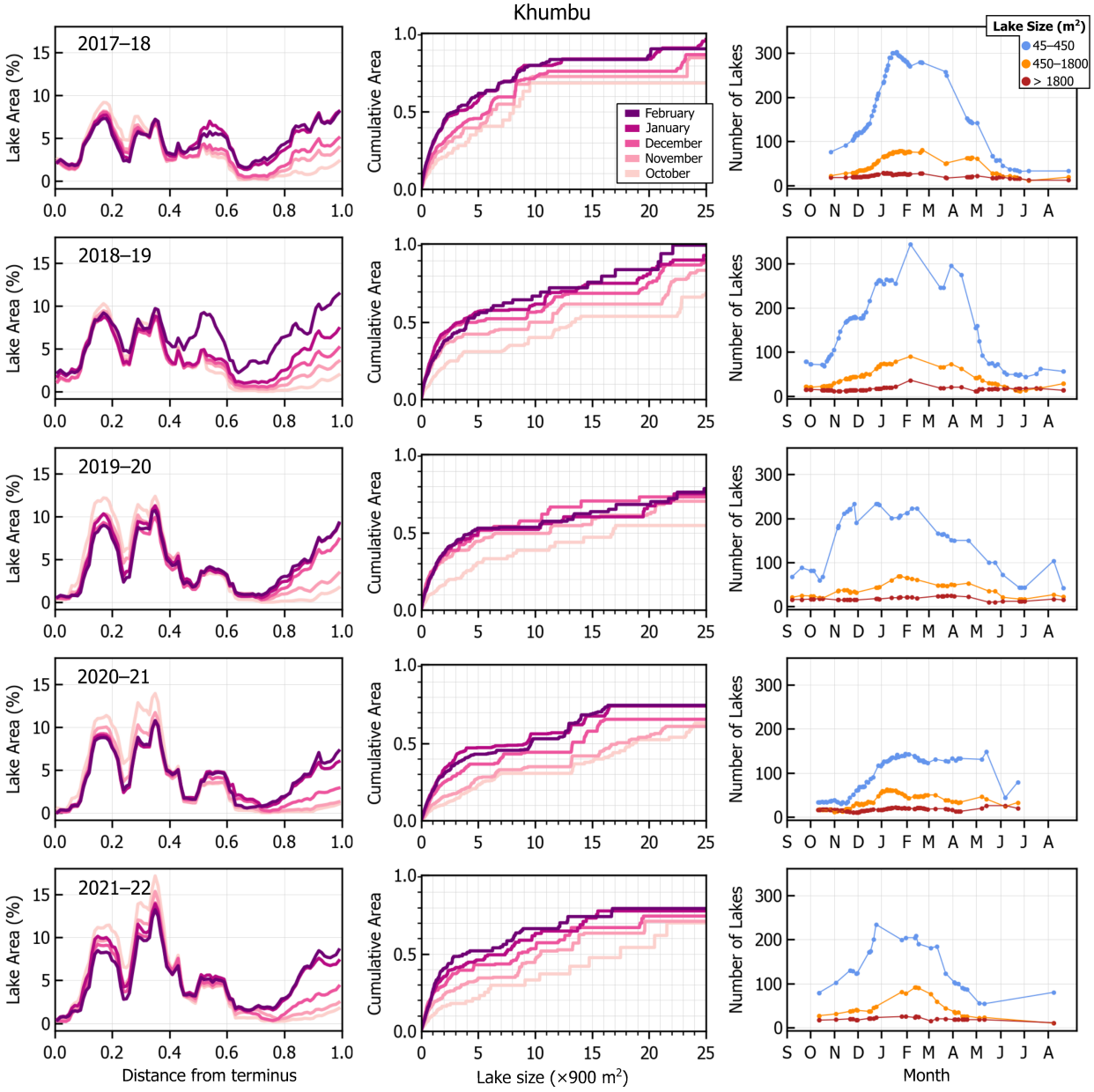

Figure S10. Seasonality in lake area and count on Khumbu Glacier, presented identically as Figure 6.

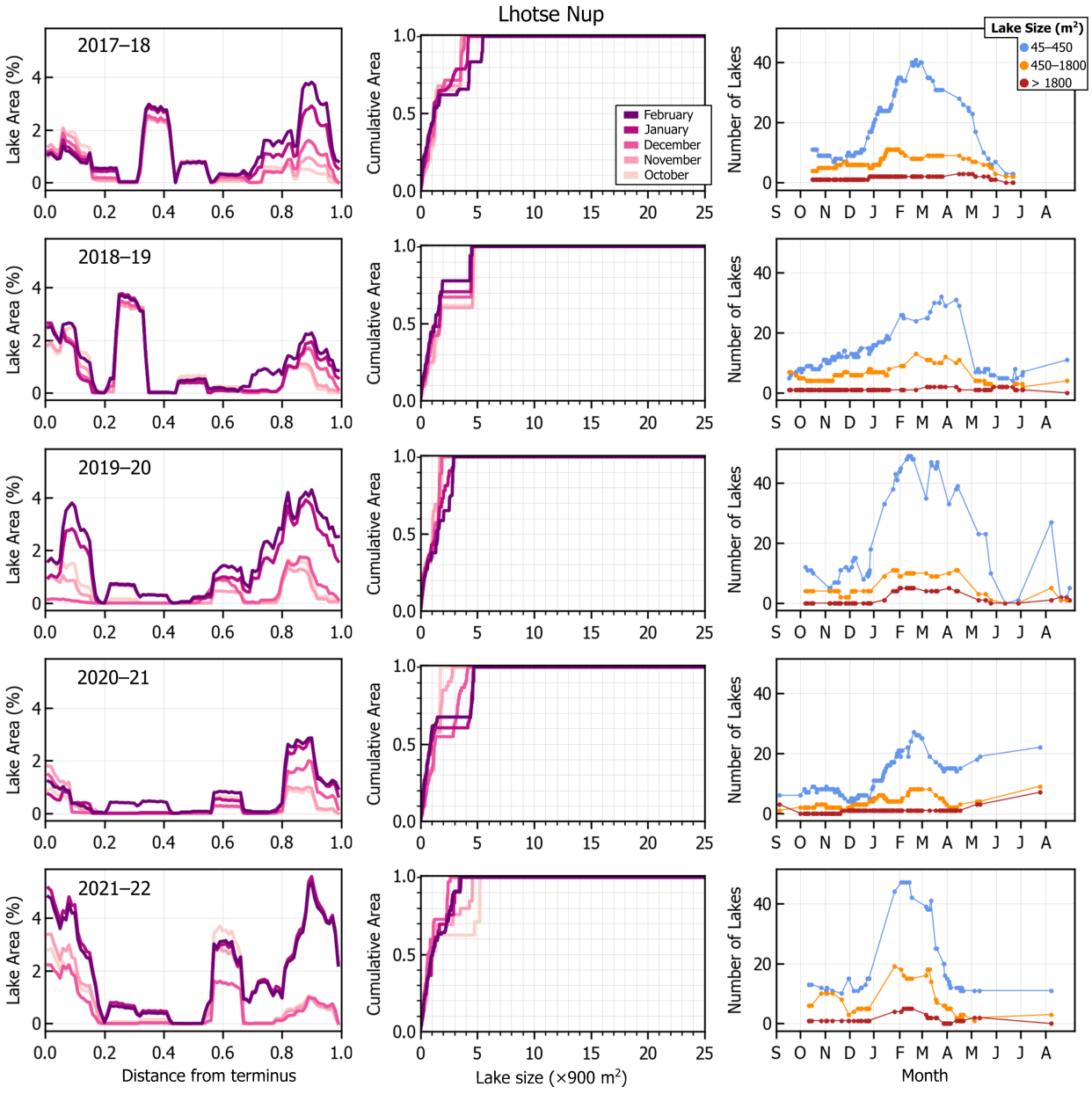

Figure S11. Seasonality in lake area and count on Lhotse Nup Glacier, presented identically as Figure 6.

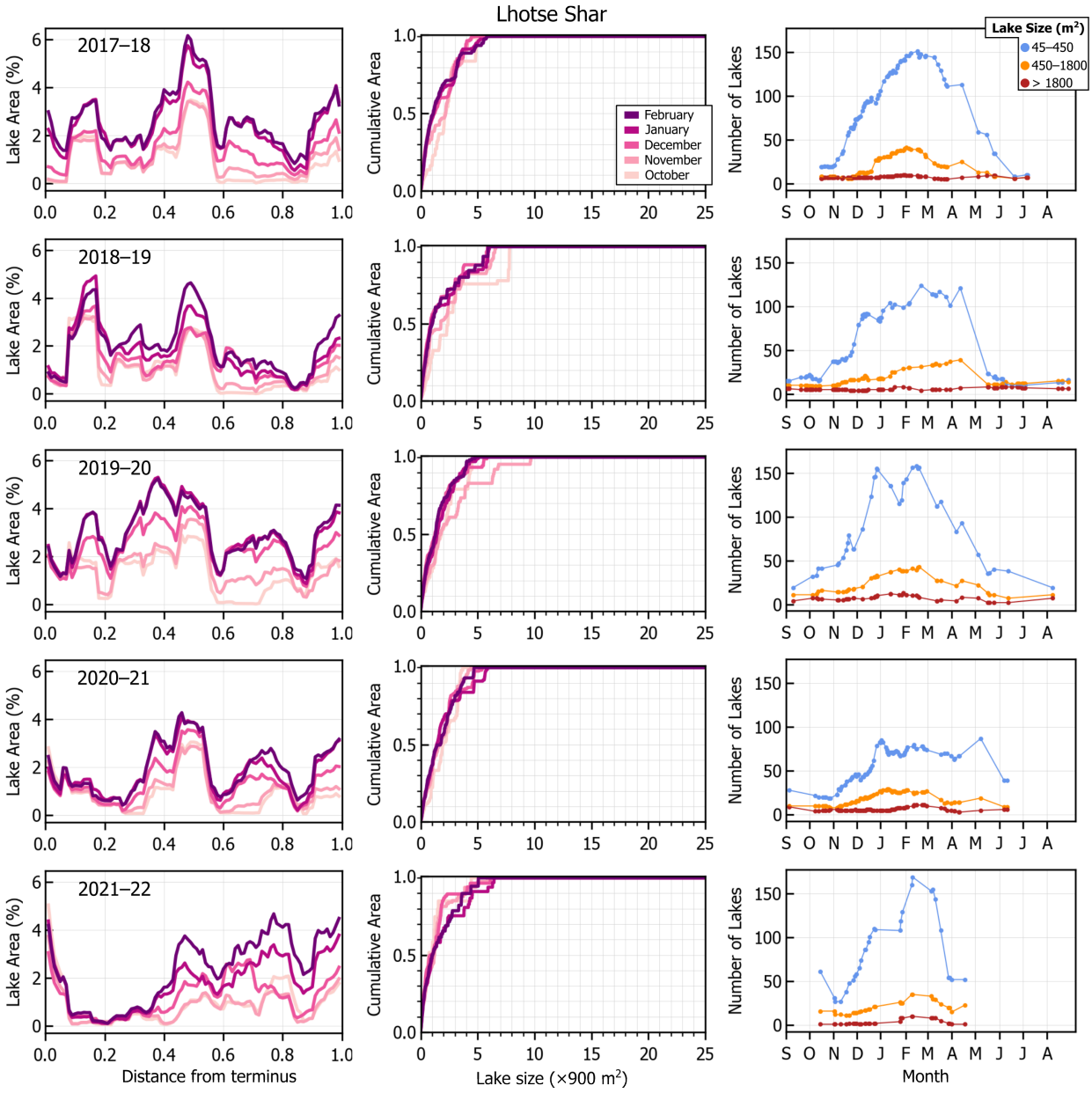

Figure S12. Seasonality in lake area and count on Lhotse Shar Glacier, presented identically as Figure 6.

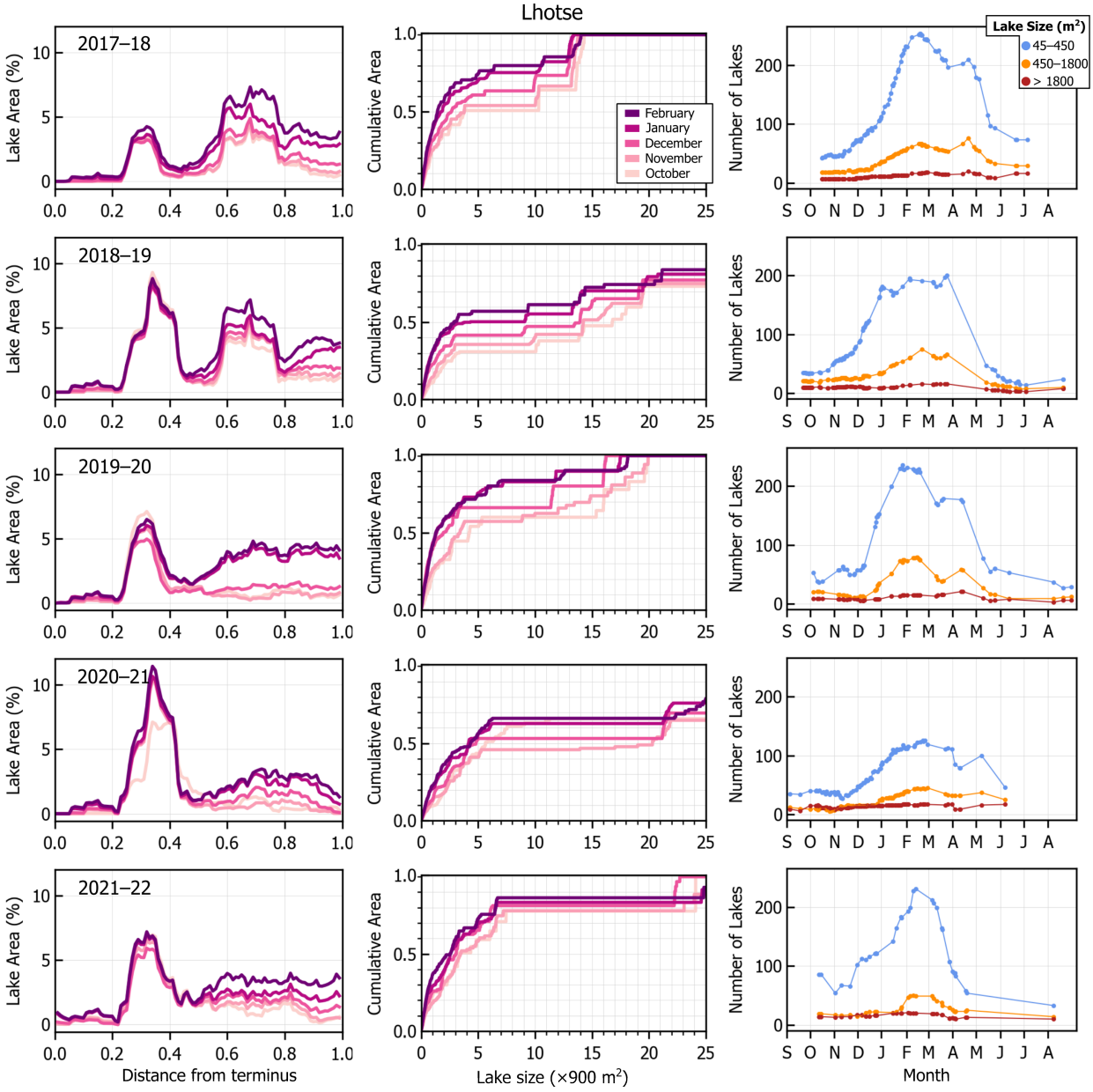

Figure S13. Seasonality in lake area and count on Lhotse Glacier, presented identically as Figure 6.

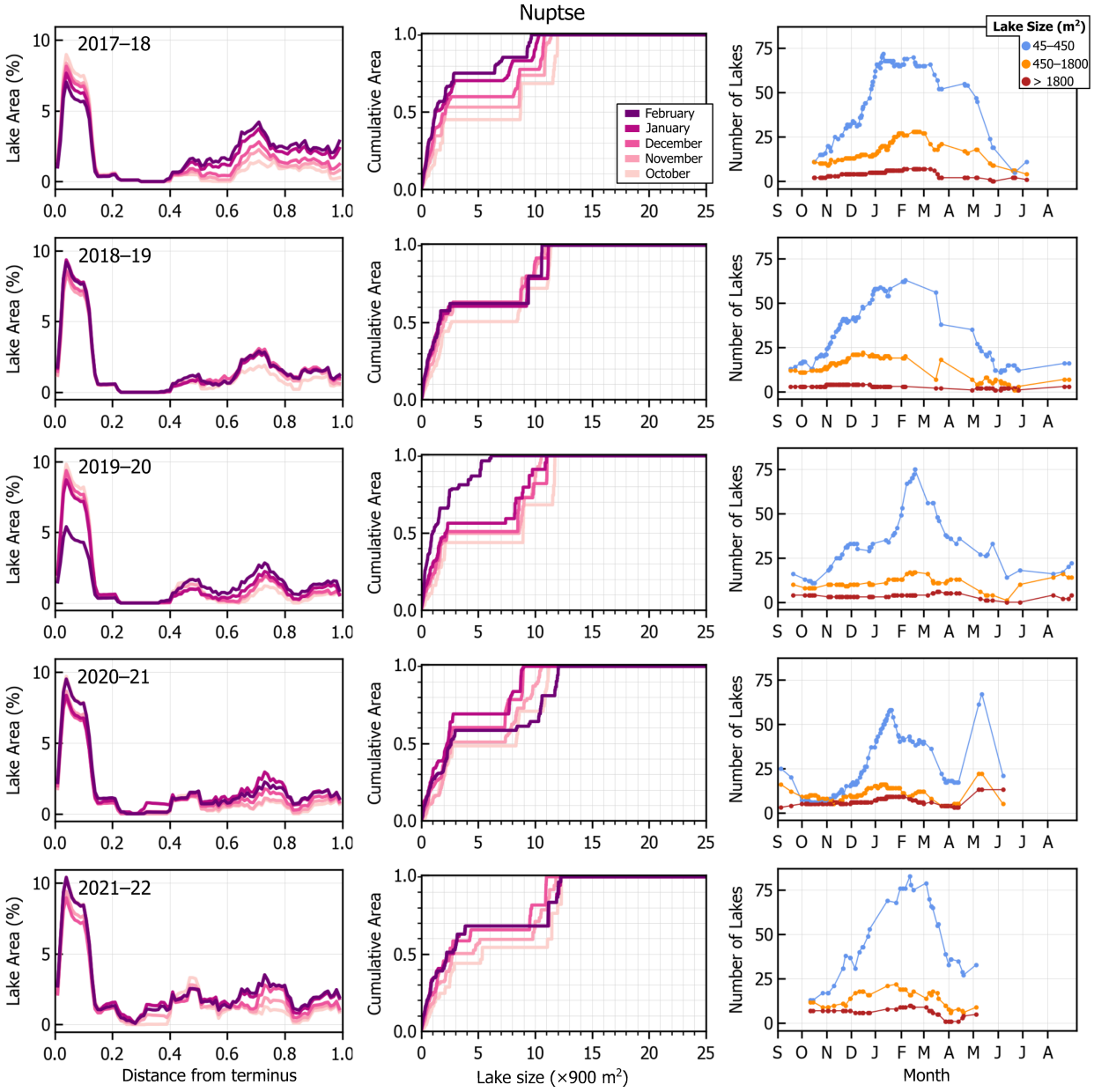

Figure S14. Seasonality in lake area and count on Nuptse Glacier, presented identically as Figure 6.

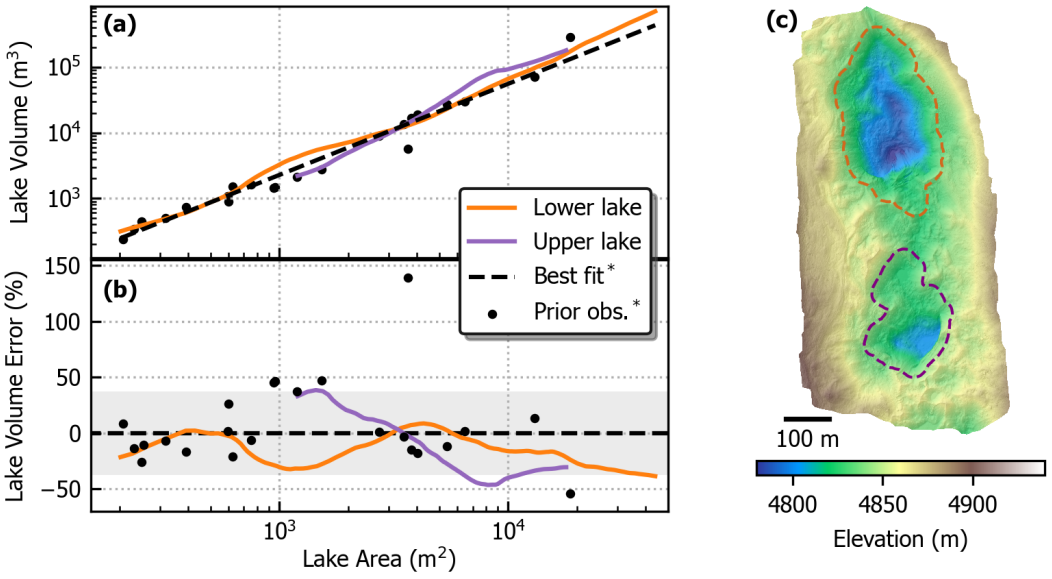

Figure S15. The area-volume scaling relationship for the two large lake basins on Ambulapcha Glacier (purple and orange lines). Black points show previous observations of SGL areas and volumes on Khumbu Glacier by Watson et al. (2018b), and the black dashed line is the best-fit relationship presented in the study. (a) shows the area-volume relationship (in log-log scale). (b) shows the percent error that results from using the best-fit equation for estimating volume from an observed area. Grey shaded area shows the 37% mean error from all observations in Watson et al. (2018b). (c) shows the UAS-derived DEM (hillshade with elevation overlaid) and approximate extents of the two lake basins.

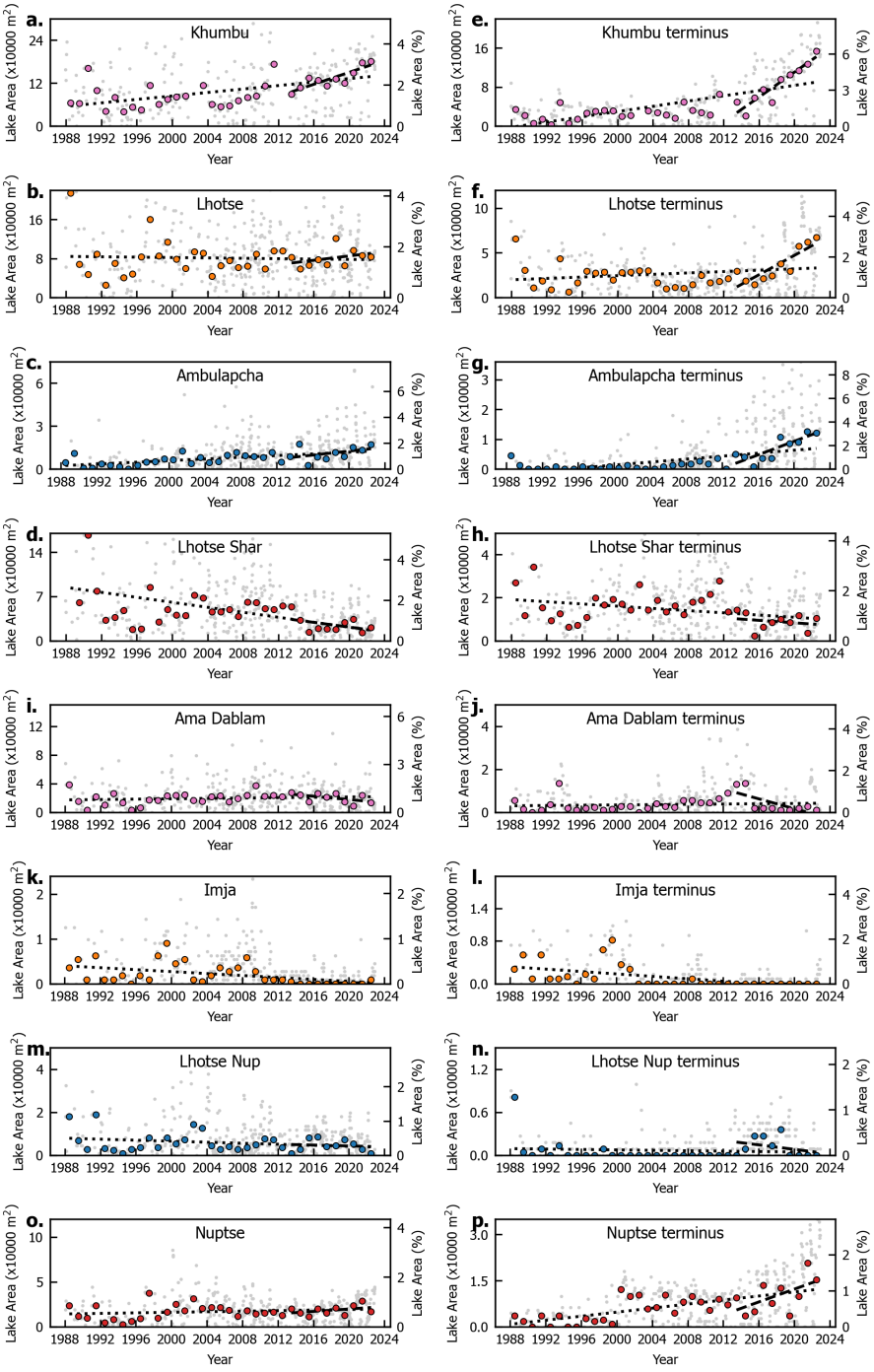

Figure S16. Landsat-derived time series of SGL area of all 8 glaciers.

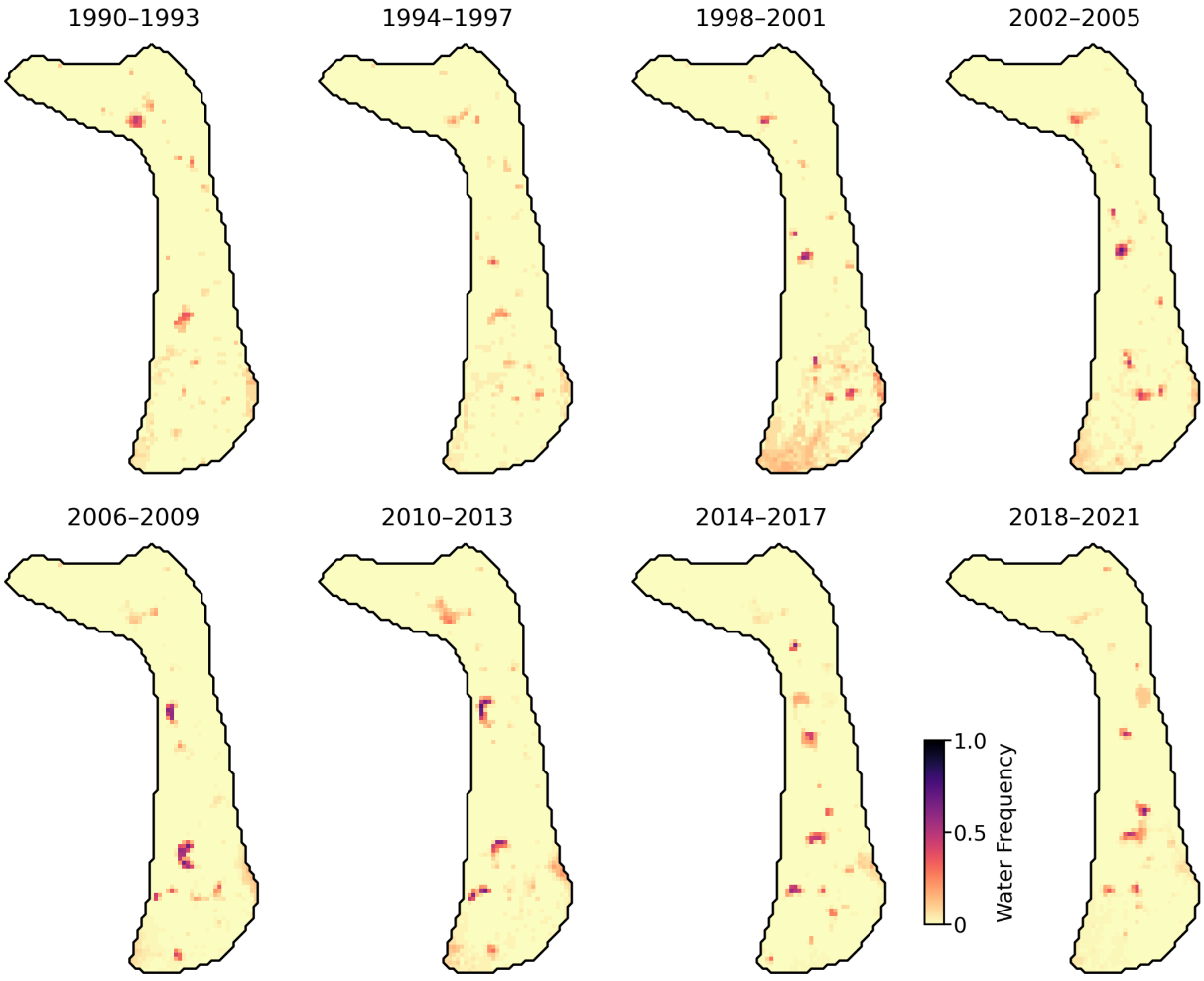

Figure S17. Repeat 4-year maps of SGLs on Ama Dablam Glacier, from Landsat imagery.

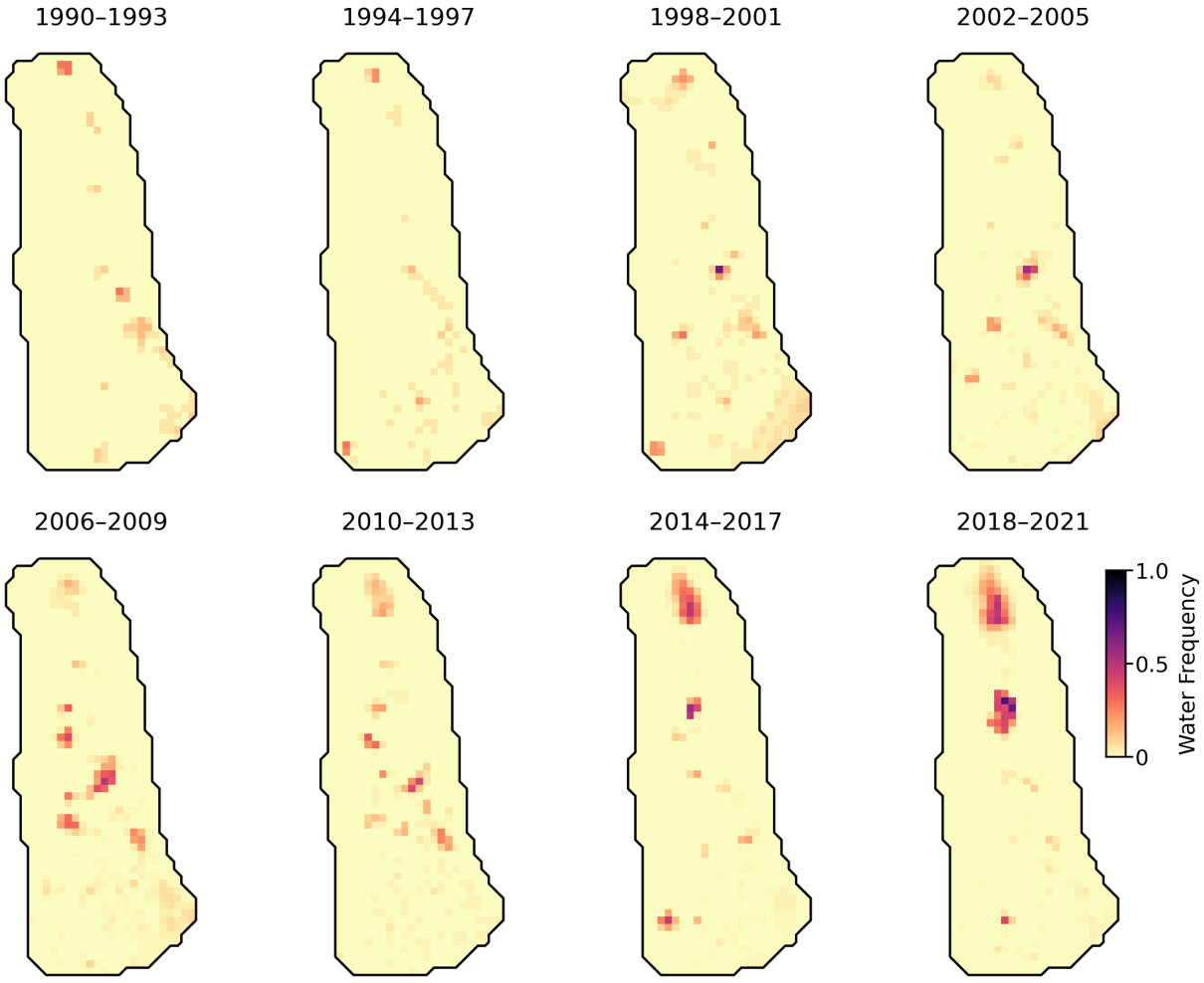

Figure S18. Repeat 4-year maps of SGLs on Ambulapcha Glacier, from Landsat imagery.

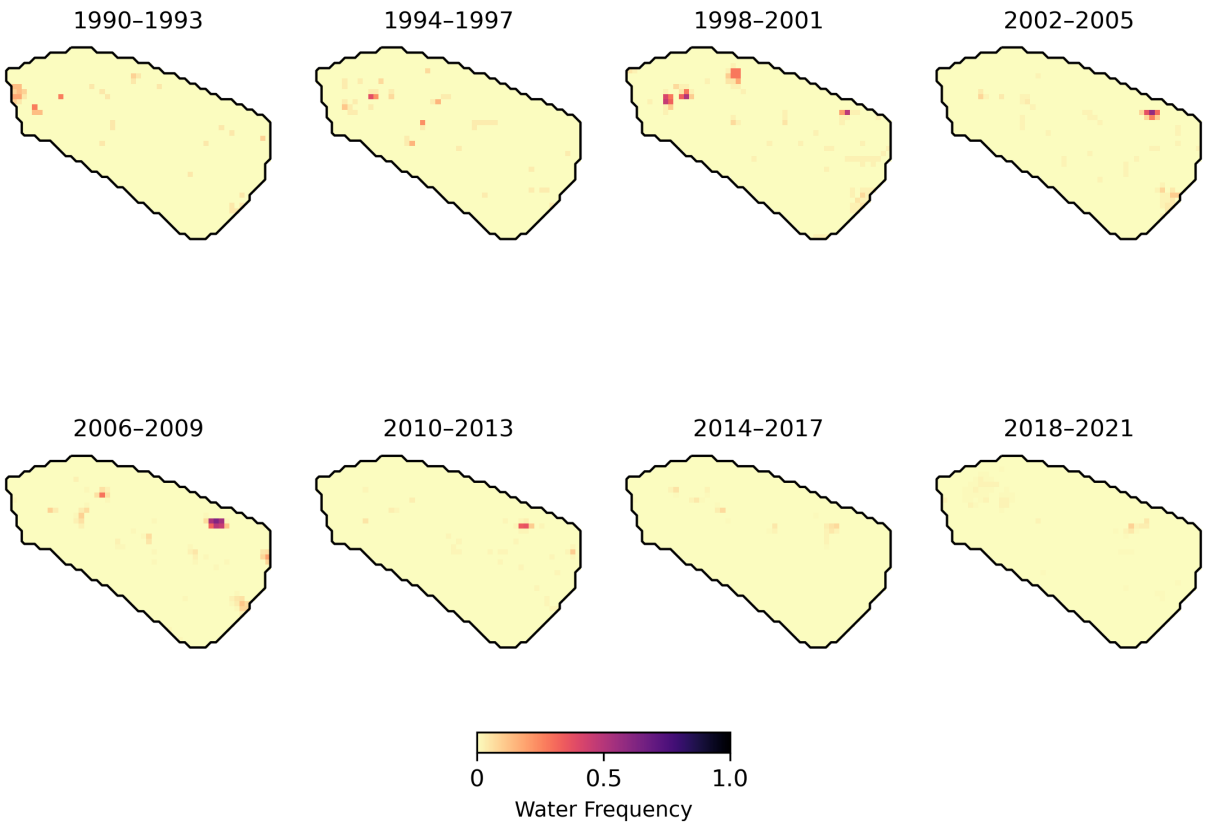

Figure S19. Repeat 4-year maps of SGLs on Imja Glacier, from Landsat imagery.

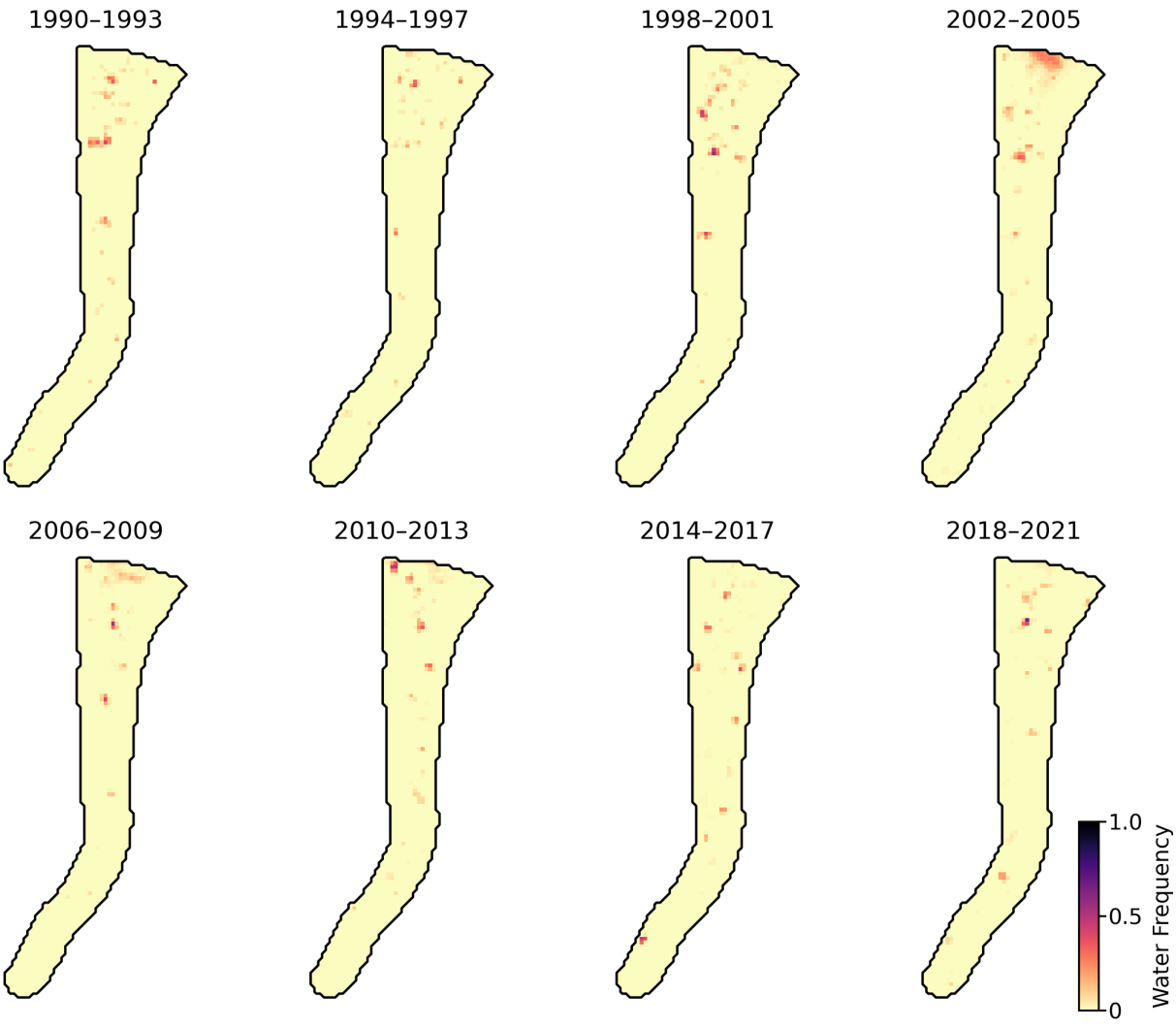

Figure S20. Repeat 4-year maps of SGLs on Lhotse Nup Glacier, from Landsat imagery.

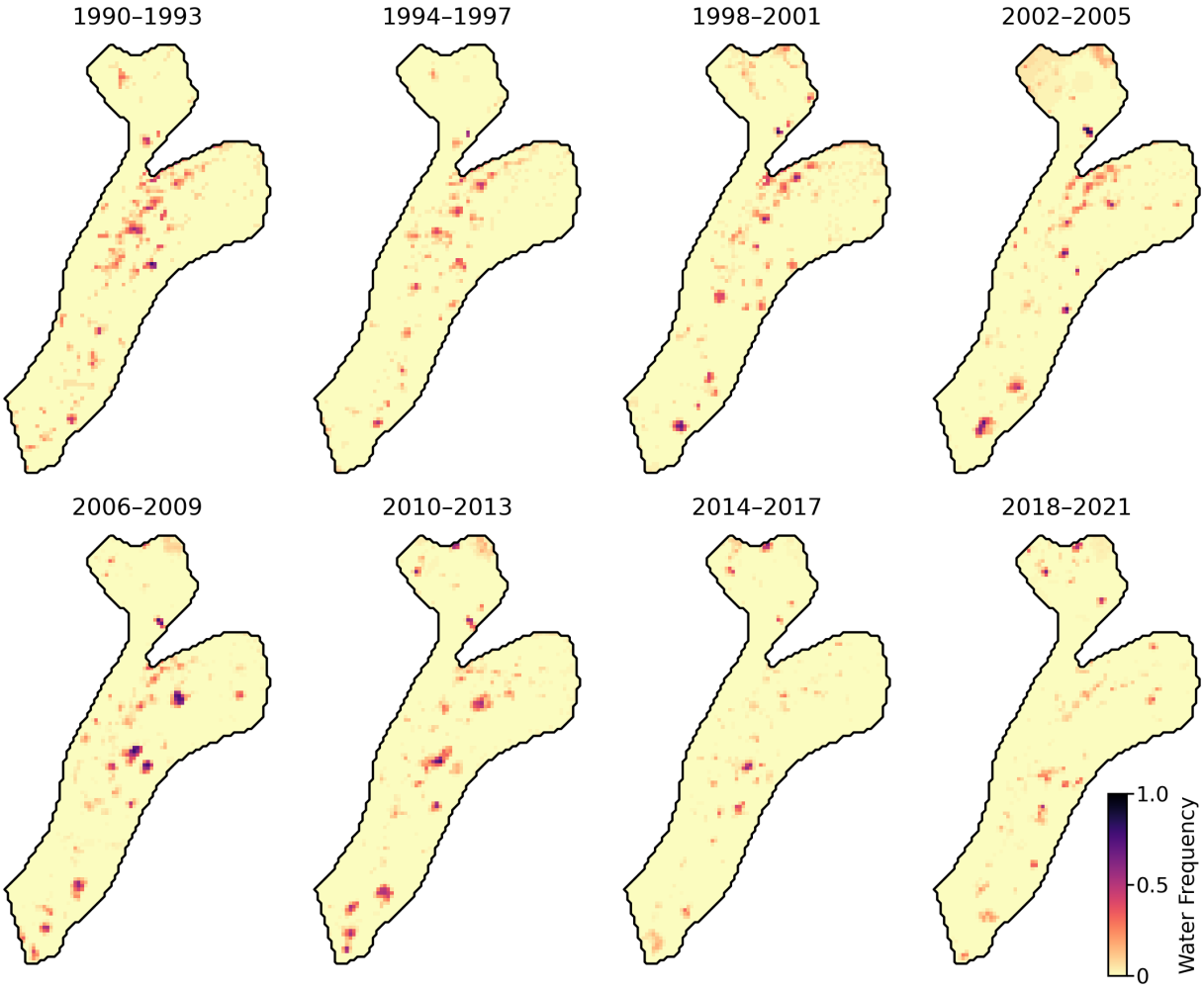

Figure S21. Repeat 4-year maps of SGLs on Lhotse Shar Glacier, from Landsat imagery.

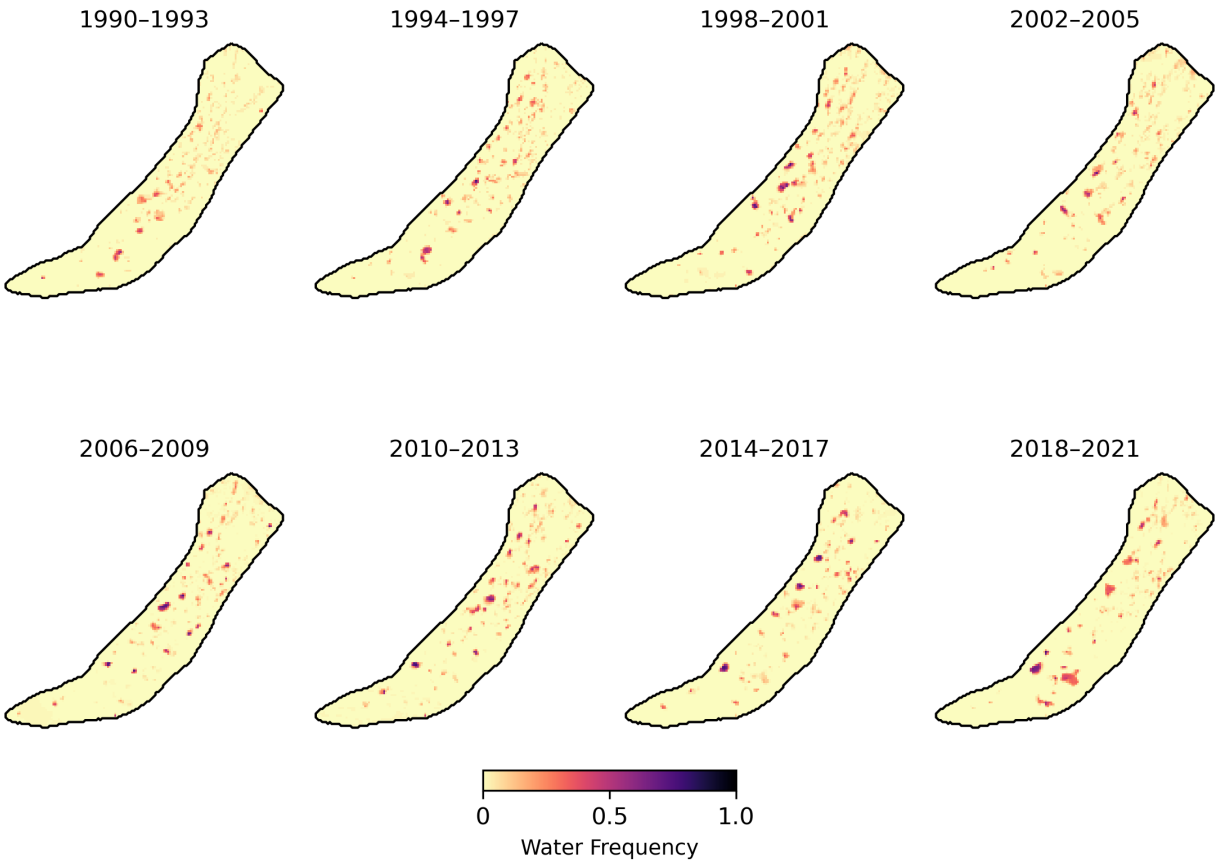

Figure S22. Repeat 4-year maps of SGLs on Lhotse Glacier, from Landsat imagery.

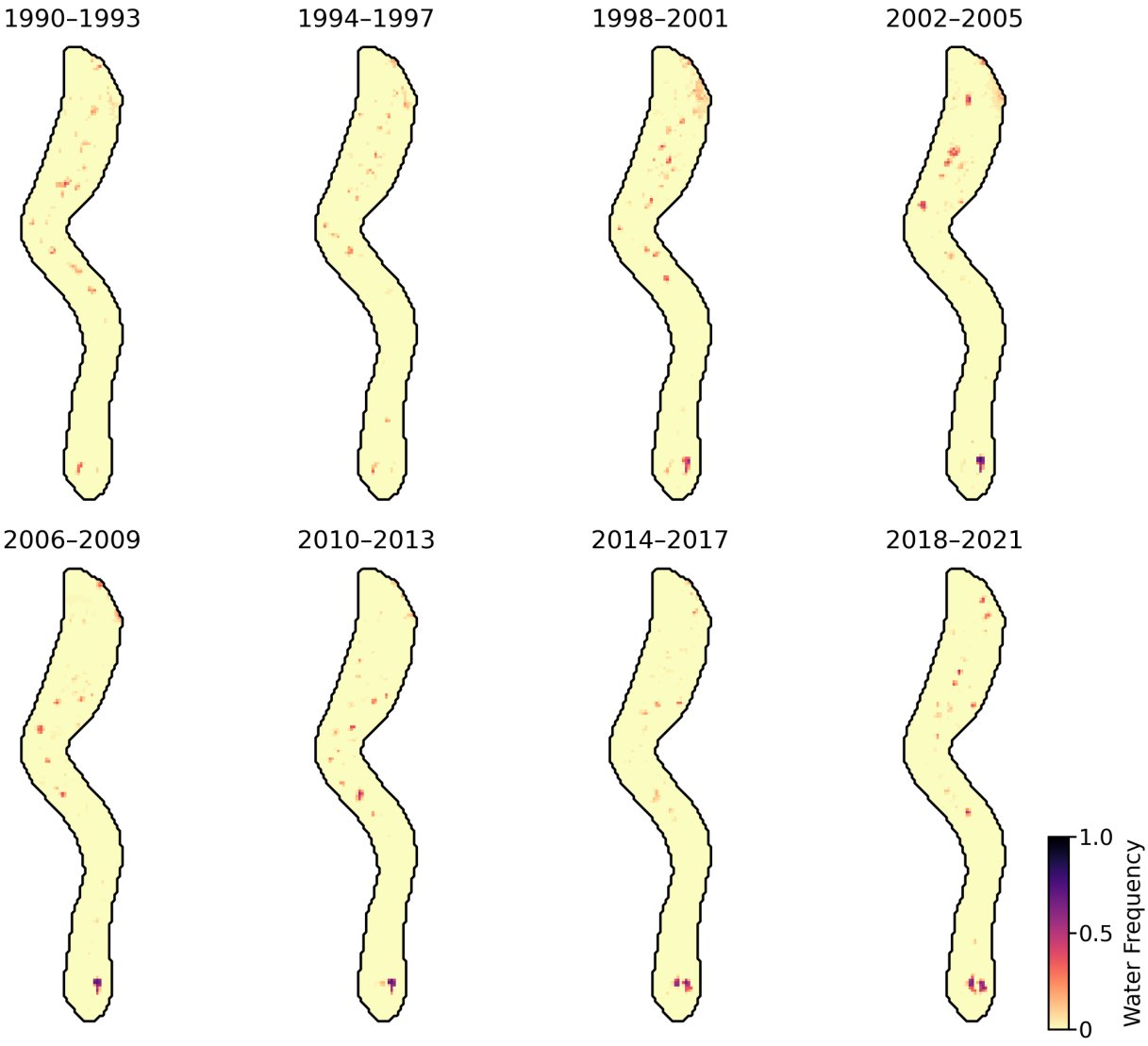

Figure S23. Repeat 4-year maps of SGLs on Nuptse Glacier, from Landsat imagery.